Impact of product gas impurities from dehydrogenation of perhydro-dibenzyltoluene on the performance of a 10 μm PdAg-membrane

Alexander Wunsch [a], Ellen Gapp [a], Thijs Peters [b], Peter Pfeifer [a,*]

[a] Institute for Micro Process Engineering, Karlsruhe Institute of Technology (KIT), 76344, Eggenstein-Leopoldshafen, Germany
[b] SINTEF Industry, P.O. Box 124, Blindern, N-0314, Oslo, Norway

Keywords:
PdAg-Membrane
LOHC
Dehydrogenation
Membrane poisoning
Hydrogen purification

A B S T R A C T

The purification of the product gas from dehydrogenation of liquid organic hydrogen carriers (LOHC) by using PdAg-membranes is highly promising, since the low level of impurities in the released hydrogen stream allows low pressure operation and favours the coupling with the dehydrogenation step. Motivated by our recent short-term investigations indicating an influence of these impurities on the membrane performance the behaviour of the membrane by exposure to product gas was investigated in detail over a long period. In total, the membrane was operated for more than 200 days, including approx. 21 days under product gas from the LOHC-dehydrogenation. In the time period the performance has decreased by 88% and could be restored slowly but completely by using pure hydrogen. The degradation is caused by the coverage of active adsorption sites for the dissociation of hydrogen by hydrocarbons other than methane. The activation energy of permeation has almost tripled from 13 kJ mol ^{1} to 38 kJ mol ^{1} while desorption of impurities from the surface affect the process and its temperature dependence. SEM-analysis of the still 100%-selective membrane after more than 200 days of operation shows no significant changes in membrane morphology. Under the mild operating conditions, a lifetime of several years seems possible.

1. Introduction

As an energy carrier, renewable hydrogen is crucial for reaching the German and global climate goals [1–3]. However, the nature of hydrogen poses great challenges for economically viable storage and transport [4]. Chemically bound to organic liquids (Liquid Organic Hydrogen Carriers, LOHC), mostly of aromatic structure, increases the handling, chemical and thermal stability, volumetric storage density and safety [5–10]. The LOHC-material system perhydro-dibenzylto luene/dibenzyltoluene (H18-DBT/H0-DBT) has already been established for commercial use, since it largely meets the selection criteria for a suitable LOHC [11,12]: commercial availability, fast dehydrogenation kinetics, low vapour pressure, low toxicity and a high cycle stability which is also related to a high stability of the organic carrier at the temperature of dehydrogenation. Dibenzyltoluene is a mixture of different stereoisomers of three toluene oligomers bound via the methyl group.

Currently, scenarios and prospective areas of LOHC application are being investigated in which the distribution of hydrogen via the LOHC technology is economically useful, technologically feasible and sustainable [13–26]. One of these scenarios is the supply of hydrogen to hydrogen refuelling stations. For the use in fuel cell vehicles, high purity hydrogen according to the ISO 14687–2 specification is required [27]. However, hydrogen from LOHC-dehydrogenation contains up to 1000 ppm of contaminants, not fulfilling the named standards [27]. The hydrogen purity is adversely affected by contaminants that originate from dibenzyltoluene production and further by decomposition and vaporization of LOHC-molecules in itself during the dehydrogenation process, which is operated at around 300 °C. In sum both impacts result in impurities of volatile hydrocarbons up to their saturation pressure in the hydrogen gas stream [27–29]. The raw material, dibenzyltoluene, which is used in technical quality, contains small amounts of low- and high-boiling contaminants including oxygenates [30,31]. As this contaminant level can exceed that occurring due to catalytic decomposition during dehydrogenation by orders of magnitude, pre- and/or post-treatment steps of the raw material are necessary. Bulgarin and colleagues have further shown that traces of water and other oxygen-containing components in the LOHC results in the formation of CO and CO_2. Furthermore, the Pt-based catalyst, identical to the one used in our study, also shows an activity for methanation, so the released

* Corresponding author.
E-mail addresses: alexander.wunsch@kit.edu (A. Wunsch), ellen.gapp@kit.edu (E. Gapp), thijs.peters@sintef.no (T. Peters), peter.pfeifer@kit.edu (P. Pfeifer).

CO_2 reacts directly to CO and CH_4 (see Ref. [32] supplementary file). With increasing pressure, the amount of CO decreases continuously while the amount of CH_4 increases. These oxygen-containing residues can be removed by outgassing/drying. Cycling the LOHC material three times in the hydrogenation-dehydrogenation process while storing it under protective atmosphere is also an option for cleaning-up the LOHC. During these initial cycles the catalyst-related productivity increases. The contaminants in the released hydrogen, however, must be removed circumstantially by activated carbon filters or pressure swing adsorption systems [27,32].

The use of Pd-based membranes could partially or completely replace these procedures and further lead to a process intensification in the dehydrogenation [29,33]. Pd-based membranes offer an almost infinite permselectivity with respect to hydrogen [34–36]. Amongst them, PdAg-membranes are possibly best suitable ones for combination with dehydrogenation, because the increased amount of Ag in the Pd-lattice can lower the α-β phase transition temperature of pure palladium to enable the operation below 300 °C [37–42]. The small amount of impurities results in a high driving force of the separation already at moderate pressure differences (1–3 bar(g)), which thermodynamically favours the dehydrogenation. A hydrogen purity exceeding 99.999% could already be achieved in our preliminary work [29].

However, it could be found that after 8 h of exposure to hydrogen contaminated with a sum of approximately 250 ppmv the hydrogen flux across the PdAg-membrane dropped significantly, but could be almost completely restored by treatment with pure hydrogen [29]. We have investigated this phenomenon in more detail in this work and want to address the following questions:

(a) How does operating time with LOHC product gas affect the degradation/regeneration of the membrane?
(b) How does degradation and regeneration affect the long-term stability of the membrane?
(c) What are the limitations of the membrane-integrated LOHC dehydrogenation process?

Several studies have already been carried out investigating the interactions between the level of other gas substances and Pd-alloy membranes. The hydrogen flux of the membrane generally decreases with increasing concentration of other "inert" substances due to reduced driving force (reduced partial pressure) and can even be limited by the mass transport towards the membrane, i.e. by so-called concentration polarisation if the hydrogen flux across the membrane is higher than the mass transport in the gas phase [43–50]. In general, the influence of dissociative adsorption of hydrogen increases with decreasing membrane thickness. At low membrane thickness, surface kinetics limitations can potentially lower the hydrogen flux and can further lead to a different dependency of the hydrogen flux on the partial pressure difference between retentate and permeate side [51,52]. Also, the temperature dependence of the hydrogen flux can change due to the increasing importance of the activation energy of dissociation versus that of diffusion in the membrane bulk [53].

The most critical issue is, however, when traces of other substances i.e. impurities are present in the feed gas that can cover the membrane surface by stronger adsorption and thus take influence on the overall rate of dissociation and the importance of surface reactions in relation to the diffusion of hydrogen in the membrane bulk. Thus, surface reactions gain in importance at even higher membrane thickness [34].

In the dehydrogenation process, it is difficult to exactly predict under which conditions degradation will take place, especially when several components with different impact on the membrane are present. Therefore, an overview with focus on relevant levels of impurities for the LOHC-process is given in the following. A particular focus is given to CO, CO_2, CH_4 and saturated hydrocarbons.

Chabot [3] could only detect a negative effect on a 250 μm thick PdAg-membrane at 0.2% CO below 200 °C, while Hou [54] observed a 10% flux decrease on a 5–6 μm thick membrane at 270 °C (1% CO). The addition of CO leads to competitive adsorption of CO and H_2, while the equilibrium is shifted in favour of hydrogen with increased temperature depending on membrane thickness. In case of a 3 μm thick Pd-membrane only temperatures above 350 °C favour full H_2-adsorption [55]. Otherwise CO may be adsorbed on the membrane surface, whereby a single CO molecule can occupy several adsorption sites accessible to hydrogen and simultaneously increase the activation energy for dissociation [56,57]. It has been reported that the hydrogen flux of the membrane decreases with decreasing temperature by exposure to CO [3,54,55,58–65]. O'Brian and colleagues [63] have found that methylene is formed besides the adsorbed CO below 250 °C, which additionally covers the surface. However, this assumes that CO dissociates, which can also happen on imperfect Pd-surfaces below 127 °C despite the high activation energy [66,67]. The addition of silver weakens the bond between CO and the Pd-surface, which makes a PdAg-membrane more resistant to CO poisoning [59,68].

Chabot [3] could only detect a significant drop in the separation performance of a 250 μm thick PdAg-membrane at 9% CO_2 below 150 °C, while Hou [54] observed no change with a 5–6 μm thick membrane above 325 °C. The degradation caused by CO_2 is significantly weaker on PdAg-membranes compared to CO and is practically negligible in the presence of CO [3,62]. In contrary it was found that CO and CO_2 poison can be equally strong if the membrane is particularly thin (1 μm) [69]. Long-term experiments show that CO_2 slowly poisons the membrane related to the formation of CO or C. In addition, the degradation of the membrane by CO_2 takes more time to regenerate than caused by CO, which suggests that CO_2 promotes the formation of carbon [61]. Gielens and colleagues have also observed this phenomenon and explained it with the weak catalytic activity of Pd for dehydrogenation. The slow reaction kinetics lead to slow but steady degradation and regeneration by the formation of elemental carbon on the surface [70].

Chabot [3] observed a reduction in the hydrogen flux of a 250 μm thick PdAg-membrane at 9% CH_4 only below 150 °C. Chen [71] found a 10% decrease in permeance at 250 °C on a 700 μm thick PdAg-membrane with 10% CH_4, which increases with rising temperature and reduces the flux by up to 25% at 450 °C. No PdC compounds were detected afterwards. Most probably, the difference between the studies lies in the steam addition, which can lead to different options of methane to react either to carbon or steam reforming products.

It has been shown that saturated hydrocarbons (ethane, propane, butane) behave similarly to methane and have a weak poisoning effect [72,73]. As soon as unsaturated hydrocarbons such as olefins (e.g. ethene, propene) are present, the permeate flow decreases more strongly [73,74] or stops as the surface is blocked completely [72]. These adsorbed species remain on the surface until they decompose or become completely hydrogenated by the present hydrogen [72,75]. While at low temperatures the adsorption of impurities at active dissociation sites is responsible for the decrease in flux, at higher temperatures the formation of coke deposits or even entire layers leads to performance losses [72,76]. The higher the temperature, the more likely deposited carbon atoms will migrate into the material and change it, which will permanently interfere with the transport of hydrogen [34]. However, Easa and colleagues [65] were able to show that the reduction in flux depends only on the components adsorbed on the surface.

The degradation is mostly reversible – the surface can be reactivated by post-treatment with air or pure hydrogen [60,61,76]. However, the structure of the adsorbed hydrocarbons evolves to become a more potent poisoning with increasing exposure time also at temperatures below 350 °C, making them more difficult to oxidize. The way the structure of the adsorbed species changes was investigated by Easa et al. - most likely coke precursors are formed [61,65].

Cyclic hydrocarbons and Pd-based membranes are mainly investigated in literature in the context of membrane reactor systems in which high concentrations of these hydrocarbons are in contact to the

membrane [75,77–87].

In contrast to literature this work specifically focuses on the impact of contaminations in extremely hydrogen-rich gas with a sum of 350 ppmv contaminants from LOHC-dehydrogenation of perhydro-dibenzyltoluene which shall be cleaned ideally to levels of sub-ppmv according to the purity requirements of hydrogen in automotive applications. The studies are performed on a 10 μm thick PdAg-membrane. The contaminants are mostly saturated and unsaturated (depending on the reaction progress) cyclic hydrocarbons. Long-term experiments, scarce in literature, have been performed to investigate the behaviour of the membrane at these low concentrations. Moreover, the permeability and permselectivity was determined at different points during these long-term experiments. At the end of the experiments the membrane surface and cross-area was analysed by scanning electron microscope (SEM).

2. Materials and methods

2.1. Membrane performance evaluation

An illustration of the applied membrane module is shown in Fig. 1. As already presented in previous work, microstructures are used for the supply of feed and permeate gaseous streams [29,33,50,80,88]. A total of 34 channels measuring 4 cm × 200 μm × 200 μm (length × height × width) are provided on each side. The PdAg-membrane (77 wt% Pd, 23 wt% Ag) used is 10 μm thick and is mechanically stabilized by two micro sieves (stainless steel, and without diffusion barrier layers) and integrated between the two foils with micro channels. The stack is then bonded by laser welding. The effective membrane area is 1.5 cm^2 [29, 80]. The growth side of the Pd-film was used as the feed side of the membrane in the module. The membrane was produced by magnetron sputtering and provided by SINTEF (Oslo, Norway) [89].

Fig. 2 shows the experimental test rig used in this study. Either nitrogen (5.0) or hydrogen (5.0) can be fed from gas cylinders to the feed side and permeate side of the membrane. The feed side can also be fed with the product gas from the dehydrogenation process of perhydro-dibenzyltoluene. The main portion of LOHC is condensed at ambient temperature prior feeding to the membrane. Thus the dehydrogenation reactor and the membrane separator are thus thermally decoupled. A more detailed description of the reactor and the reaction system can be found in Refs. [29,33]. The pressure can either be controlled by an automated pressure retention valve (PIC) or manually by a needle valve. Retentate and permeate flow can be measured together or separately in a soap film flow meter (SFFM) manually, while their composition is analysed by gas chromatograph. Furthermore, a mass flow meter (MFM, 0–2 NL min^{-1}) calibrated with pure hydrogen in range from 5 to 500 NmL min^{-1} has been added for continuous monitoring of the streams with an accuracy of ±0.1 NmL min^{-1}.

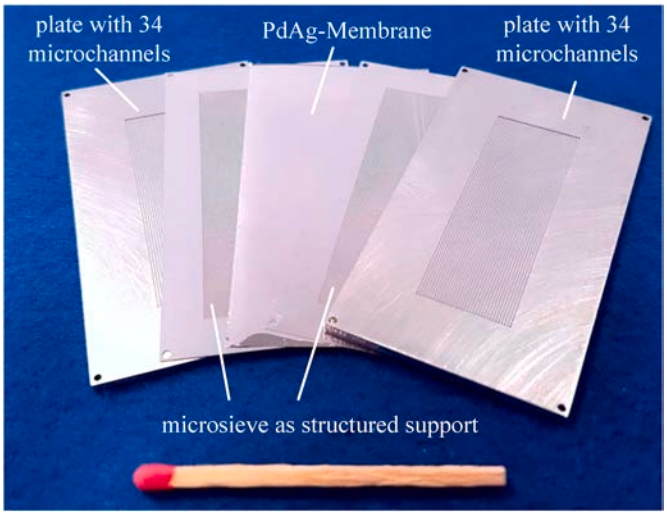

Fig. 1. Structure of the microstructured membrane module.

2.2. Product gas analysis

The analysis of the product gas was performed using a gas chromatograph (Agilent 6890A, Agilent Technologies Deutschland GmbH, Germany) with an FID-TCD combination. A column system, consisting of a non-polar column (HP-1) for hydrocarbons, a HP-Plot Q for H_2O and CO_2, and a molecular sieve (HP-Plot 5A) for the permanent gases CO, N_2, O_2, was used. As carrier gas hydrogen 5.0 was used on all columns. On the FID methane was calibrated and for all other hydrocarbons the calibration of methylcyclohexane was used as conversion factor.

2.3. Long-term experiment

Initially, the membrane was heated up to 300 °C under nitrogen atmosphere (450 NmL min^{-1}) at a rate of 1 K min^{-1}. Subsequently, the long-term experiment was started with hydrogen feed (450 NmL min^{-1}) and pressure increase to 4 bar on the retentate side. A timeline of the more than 200-days experiment is shown in Fig. 3. The conditions applied to the membrane are divided in several periods and the respective parameters are listed directly under the timeline.

In section ① the membrane was operated with pure hydrogen at 4 bar for 46 days. After 360 h the permeances were determined between 300 and 340 °C. The permeance Π is the proportionality coefficient of flux ($\dot{F}_{H_2}$) and hydrogen partial pressure (p_{H_2}) difference between the retentate and permeate side (see equation (1)). Using the measured flux at different retentate pressures, a linear regression for a constant Sieverts-exponent n can be applied with the slope being the permeance at constant temperature. For better data agreement, the Sieverts-exponent n was first adjusted [34,35,52,90].

$$\dot{F}_{H_2}\left[\frac{\text{mol}}{\text{m}^2\ \text{s}}\right] \quad \Pi \quad \left(p^n_{H_2,\text{Ret}} \quad p^n_{H_2,\text{Perm}}\right) \tag{1}$$

The permeance is defined as the quotient of the material-specific permeability Q and the membrane thickness s (see equation (2)). The temperature dependence of permeability can be expressed by the Arrhenius approach. Using the permeances at different temperatures (T in K), the activation energy E_A and the pre-exponential factor Q_0 were obtained. R corresponds to the universal gas constant [34,35,52,90].

$$\Pi\left[\frac{\text{mol}}{\text{m}^2\ \text{s}\ \text{Pa}^n}\right] \quad \frac{Q}{s} \quad \frac{Q_0 \exp\left(\frac{E_A}{R\ T}\right)}{s} \tag{2}$$

This procedure was repeated after 936 h and compared with the previous measurement. After 768 h a permselectivity measurement was performed to check for a potential leakage of the membrane. For this purpose, pure gas experiments with hydrogen and nitrogen (as inert component) were carried out at a feed flow of 450 NmL min^{-1}. Both permeate streams were measured manually by soap film flow meter. The ideal permselectivity S (see equation (3)) is the ratio between the permeate flows of pure hydrogen and pure nitrogen at identical pressure difference and temperature [50].

$$S\ [\ ]\quad \left.\frac{\dot{V}_{H_2}}{\dot{V}_{N_2}}\right|_{p,\ T} \tag{3}$$

In our previous work, the membrane was operated with product gas from hydrogenation for single periods of 8 h per day [29]. In contrast to this, a 24 h overnight experiment (see section ②) was attached directly after section ①. In section ③, pure hydrogen was again fed to the membrane for 10 days to study the regeneration behaviour after this

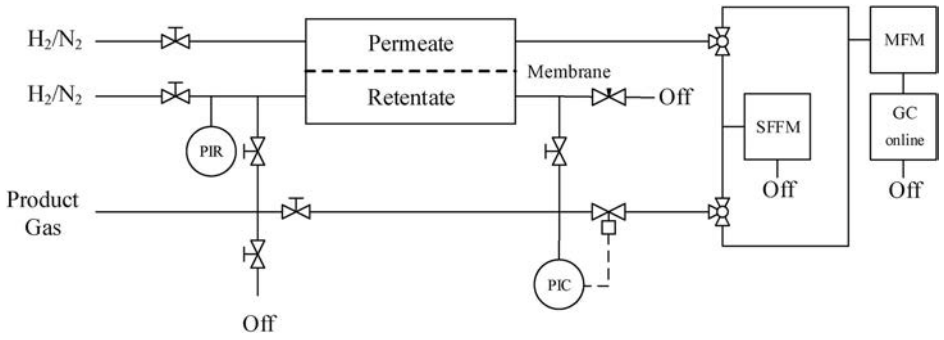

Fig. 2. Simplified flow diagram of the membrane test rig. A more detailed illustration can be found in our previous publication [29].

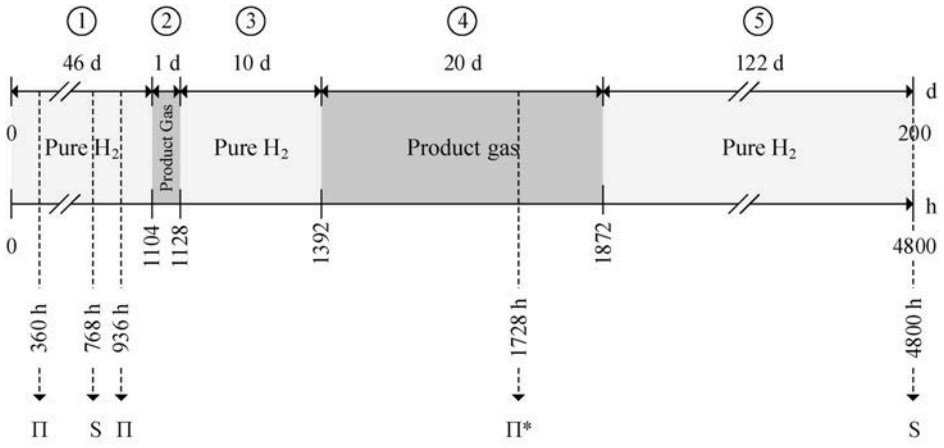

① Hydrogen, $\dot{V}$ = 450 NmL min^{-1}, T = 300 °C, p_{Ret} = 4 bar, p_{Perm} = 1 bar = constant

② Product gas, $\dot{V}$ = 30 - 35 NmL min^{-1}, T = 300 °C, p_{Ret} = 4 bar

③ Hydrogen, $\dot{V}$ = 450 NmL min^{-1}, T = 300 °C, p_{Ret} = 4 bar

④ Product gas, $\dot{V}$ = 30 - 35 NmL min^{-1}, T = 300 °C, p_{Ret} = 4 bar

⑤ Hydrogen, $\dot{V}$ = 450 NmL min^{-1}, T = 300 °C, p_{Ret} = 4 bar

Π Permeance Measurement: Hydrogen, $\dot{V}$ = 450 NmL min^{-1}, T = 300 – 340 °C, p_{Ret} = 2 – 4 bar

Π* Permeance Measurement: Product gas, $\dot{V}$ = 25 NmL min^{-1}, T = 300 – 340 °C, p_{Ret} = 4 bar

S Permselectivity Measurement: Nitrogen, $\dot{V}$ = 450 NmL min^{-1}, T = 300 °C, p_{Ret} = 4 bar

Fig. 3. Timeline of the long-term experiment over a period of 200 days. The permeate pressure (p_{Perm}) was held constant at 1 bar. Other symbols: membrane temperature T; retentate pressure p_{Ret} and volume flow $\dot{V}$.

extended exposure to hydrogenation product. In section ④, the membrane was continuously operated 24 h a day with product gas over a period of 20 days. After 14 of these 20 days (after 1728 h), the temperature was first increased daily by 10 K up to 340 °C at a constant system pressure of 4 bar, and finally set back to the initial temperature of 300 °C. As a function of the Sieverts'-exponent n (determined in the section ①), the measured flux was fitted to equation (1) as linear function for each temperature. The permeances were read off from the slope. From the permeances, the activation energy of the membrane transport, according to equation (2), was finally calculated under real conditions, i.e. product gas from LOHC dehydrogenation. During the operation with product gas the hydrogen recovery factor X_{H_2} was calculated by the ratio of permeate ($\dot{V}_{Perm}$) and feed ($\dot{V}_{Feed}$) flow.

$$X_{H_2}[\quad] \quad \frac{\dot{V}_{Perm}}{\dot{V}_{Feed}} \tag{4}$$

In the last part of the long-term experiment, the membrane was treated with pure hydrogen over a period of 4 months. At the end (after 4800 h) the permselectivity was measured again. In total the membrane module was thus operated for 200 days.

3. Results and discussion

3.1. Permeance measurements

Fig. 4 shows a Sieverts' plot of the permeance measurement after 360 h time-on-stream with pure hydrogen. As expected, the H_2 flux is observed to increase with both pressure difference and temperature. A value of 0.875 was determined for the Sieverts' exponent, which is in good agreement with the value in Ref. [29]. The hydrogen transport through the membrane is inhibited by surface reaction, which is normally seen during start-up and before full activation. It is noticeable that the pre-exponential factor is about 4 times higher in this work compared to Ref. [29], as can be seen in Table 1. For better comparability, the

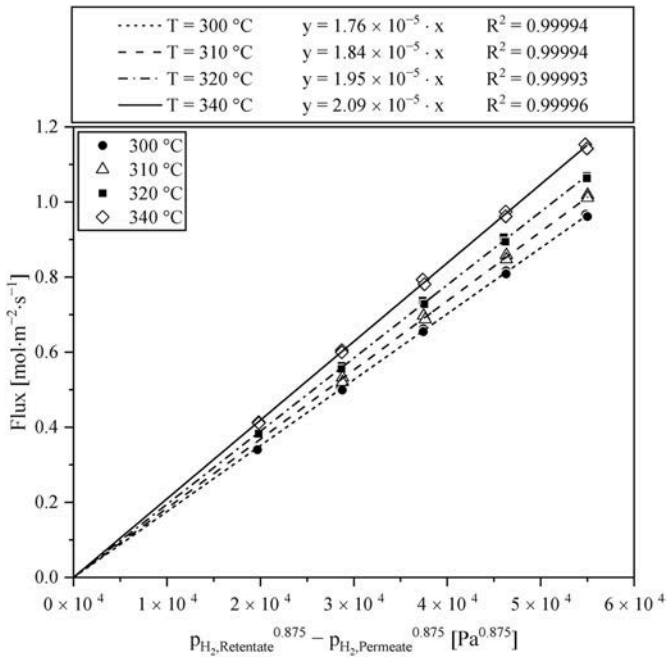

Fig. 4. Sieverts' plot of the permeance measurement after 360 h time-on-stream with pure hydrogen (450 NmL min ^{1}) as a function of temperature with a fitted Sieverts' exponent of 0.875.

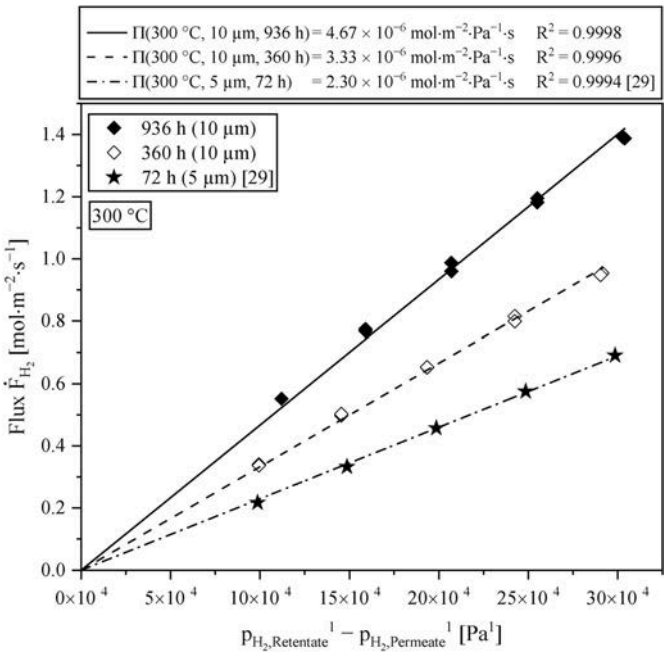

Fig. 5. Sieverts' plot of the flux at 300 °C after 72 h [29], 360 h and 936 h.

Table 1
Comparison of the characteristic membrane parameters with the previous work.

Fit for n 1	$E_{A,M}$[kJ·mol ^{1}]	Q_0[mol·m ^{1}·Pa ^{n}·s ^{1}]
[29] after 72 h (s 5 µm)	11.67	1.33 × 10 ^{10}
This work after 360 h (s 10 µm)	13.14	5.29 × 10 ^{10}

Sieverts' exponent shown in Table 1 was forced to 1 for all determined membrane parameters. The measurements differ only in the time-on-stream (72 h vs. 360 h tos). For this reason, a further permeance measurement was carried out after 936 h. The obtained results are plotted in Fig. 5. After 360 h the permeance of the 10 µm thick membrane is already 45% higher and after 936 h even twice as high as the permeance of the 5 µm thick membrane [29] after 72 h. This indicates that the membrane was not yet in a steady-state at 360 h and therefore not fully activated at this time according to Ref. [91]. The activation process takes place through the incorporation of hydrogen into the Pd-lattice, which removes contaminants. The high temperatures also can cause a change in the microstructure through grain growth and recrystallization as indicated in Refs. [34,92]. In addition, the pressure application on the PdAg-membrane retentate side causes deformation of the membrane into the holes of the micro sieves towards the permeate channels. This would result in an increase in the effective membrane area, combined with a slight decrease in membrane thickness. After about 1000 h Peters and colleagues report about an almost constant flux for a 10 µm thick Pd–Ag membrane integrated in a micro-configured module with 1 mm wide channels [89,91]. However, the temperature in their study was significantly higher (500 °C), which is a further indication that the flux may even continue to increase at our conditions after 936 h tos. An increase in flux is also possible due to the formation of defects and pinholes, which in the worst case can lead to rupture of the membrane. However, from the conclusion of the discussion on the measured permselectivity later in section 3.4, it seems not possible that the formation of pinholes has created such large effect on the hydrogen flux. Literature also indicates that when operating below 5 bars (as in this work), at least 50 days of continuous operation are possible without an effect of pinholes [89,91].

It has been reported that short-term treatment with oxygen or air ensures complete (re)activation of the membrane and the flux can be increased threefold [60,87,93–99] and thus reduce the required time for reaching steady state of the hydrogen flux. For reasons of comparability with previous work, treatment with oxygen was not considered in the current experimental series. Nevertheless, it could be introduced in the next experiments to speed–up the ramping-up phase.

3.2. Product gas impurities

The LOHC was dehydrogenated without prior treatment at 330 °C and 4 bars with an initial degree of dehydrogenation of 9.3%. The product gas fed to the membrane module consists only of hydrogen and the determined impurities as shown in Table 2. The species are divided in methane, hydrocarbons other than methane (further called only "hydrocarbons"), CO and CO_2. Overall, the impurities of 300–350 ppmv are significantly lower than in the observations from Ref. [28] (0.1–0.6%), which is probably related to our catalyst. To suppress decomposition reactions the catalyst was pre-treated with sulphur, to deactivate particularly active Pt-sites and acidic sites on the support [100]. Compared to our previous work [29], the detected contaminant level is about 100 ppmv higher. The reason for this higher level may be caused by a different batch of the LOHC with different starting degree of dehydrogenation. The higher degree of dehydrogenation (9.3%), which means the higher content of unsaturated compounds, could imply that slightly more LOHC is decomposed at the catalyst and thus ultimately more low-boiling hydrocarbons are found in the gas. Besides, the change of the GC carrier gas from argon to hydrogen compared to previous work, has enabled better detection of CO. Nevertheless, the measured

Table 2
Impurities in the hydrogen stream from the dehydrogenation of perhydro-dibezyltoluene at 330 °C and 4 bar(a), measured with GC-FID and -TCD. The degree of dehydrogenation of the starting material was 9.4%.

Methane (CH_4)	Hydrocarbons without Methane (C_7-equivalents)	CO	CO_2
40–50 ppmv	230–270 ppmv	10–20 ppmv	Not detected

CO values are not far from measurement noise and should therefore be interpreted with care even though the values for CO are in good agreement with the values of Luschtinetz [28], but higher than those of Bulgarin [32]. Differences can occur due to the content of oxygen-containing components in the starting LOHC material, but also due the reaction temperature. No CO_2 could be detected during the whole test period, which may be explained by the increased methanization activity with increasing pressure. Methane is found as a decomposition product of the LOHC and from the methanation of CO_2/CO in a concentration of 40–50 ppmv in the product gas. Note that the concentration of impurities at the membrane will drastically increase while separating a large amount of hydrogen as function of the length of the feed channels above the membrane. The goal is to utilize as much as possible of the released hydrogen from the dehydrogenation.

3.3. Long-term membrane penetration with product gas

The flux and the hydrogen recovery factor during the long-term exposure of the membrane with product gas (see Fig. 3, section ④) is shown in Fig. 6. At the initial time of operation (TOS 1400 h), the product gas flow is recovered completely until the flux drops from 35 NmL min^{-1} to 19 NmL min^{-1} within 25 h. Only in the initial first few minutes (approx.. 10 min) a dead-end mode occurs as the permeate flow is identical to the feed stream which generates an initial high concentration of impurities across the membrane; right after these few minutes the flow is divided in retentate and permeate and the impurity concentration immediately decreases. From then on, the mean concentration of impurities remains a factor of less than 5 higher than the feed concentrations. The initial decrease in permeate flow is due to the impurities in the product gas interacting with the membrane surface. The immediate surface adsorption of these substances blocks active sites for the adsorptive dissociation of hydrogen molecules. Then the flux decreases linearly until it reaches approx. 10 NmL min^{-1} after 480 h (70%). An intermediate temperature variation by 40 K, indicated by the hatched region in Fig. 6 does not change this trend. The gradual further decrease in flux can be explained by coke formation over time. However, it remains unclear which of the substances listed in Table 2 are mainly responsible for this degradation. If the components are examined separately, the influence of CH_4 in the presence of CO is negligible [3]. There are no literature data available concerning low concentrations of CO. Based on the available data, however, it is questionable whether CO has any influence at all at this low concentration at a temperature of 300 °C, since Hou observed a decrease in flux <5% at a concentration of 1% CO on a 5–6 μm thick PdAg-membrane firstly at 275 °C [54]. As the drop in performance in the presence of CO decreases with increasing temperature and decreasing concentration, a much smaller decrease in flux than 5% can be expected [3,54,55,58–65]. At 300 °C, the temperature is too high for the formation of methylene to occur on the surface and too low for elemental carbon to be deposited on the surface within a short time [54,55,63,65]. Apparently, the group of hydrocarbons (without methane) must be responsible for the gradual degradation. The group contains low-boiling and mostly mono-cyclic hydrocarbons, which are already present in the starting material or are by-products of the reaction, and residual partial LOHC, which is not completely condensed out [27]. Within the low-boiling hydrocarbons, it has been shown that unsaturated hydrocarbons in particular can lead to a significant reduction in performance [73,74]. The interactions of the membrane with cyclic compounds are of particular interest here and were investigated in preliminary work especially in connection with the dehydrogenation of methylcyclohexane in membrane reactors [80–82]. In the methylcyclohexane process, solid carbon residues on the membrane could be detected [101].

Considering that the permeate flow of 235 NmL min^{-1} (later in Fig. 10 and Fig. 11), immediately before the switch to product gas, is almost 10-times higher than the feed flow of the product gas, one would expect that despite pressure control, the retentate pressure would inevitably drop during switching. However, this could not be observed, which suggests that the impurities have made most of the membrane surface inaccessible to hydrogen within a very short time. The large drop of permeate flow at the beginning (Figs. 6 and 1400 h–1425 h) could be attributed to the adsorption of hydrocarbons molecules, since the poisoning effect of the other impurities is rather small or insignificant at these low concentrations as discussed before. In the period of further gradual decrease in permeate flow by coke formation should be considered as the hydrocarbons, once adsorbed, tend to decompose. At reducing flow rate across the membrane an established adsorption-desorption equilibrium of these species is unlikely the reason for a reduced decrease of permeate flow after 25 h of operation with product gas. We also don't believe that in the initial exposure time the high residence time increases the poisoning effect of the species as reported elsewhere [55]. As concentration polarisation is excluded in our study it is unlikely that it could cover over further membrane inhibition after 25 h of operation with product gas. We therefore hypothesize that these are two different mechanisms of degradation and that coke formation is an underlying effect from the beginning and becomes significant in the period >1450 h.

As reported in Fig. 3, the long-term product gas penetration (shown in Fig. 6) is already the second product gas run. After the first product gas run with 24 h duration the membrane got regenerated by the following 10 d hydrogen exposure, but the flux was not fully recovered (around 80%, see later in Fig. 10). To find out, if the partial deactivation of the membrane after the first run influences the initial deactivation of

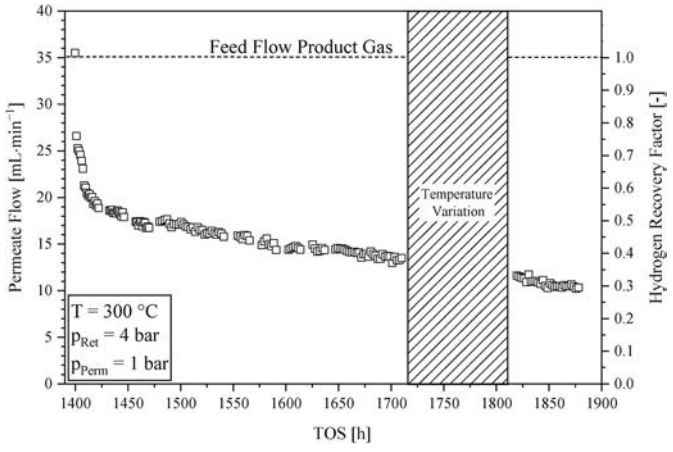

Fig. 6. Permeate flow and hydrogen recovery factor of the membrane, fed with 25 NmL min^{-1} product gas over a period of 480 h at 300 °C and 3 bar(g).

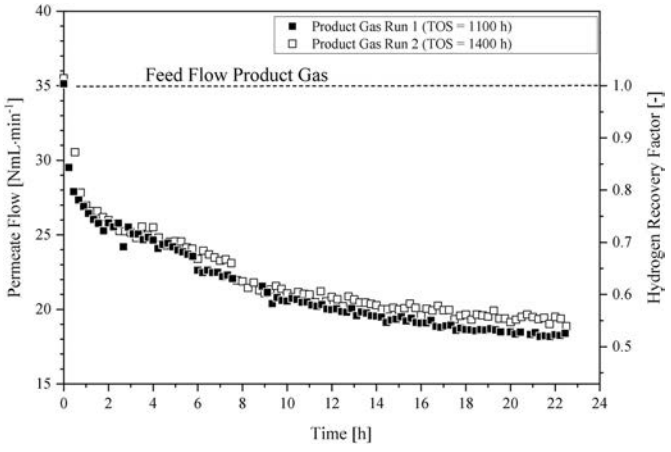

Fig. 7. Comparison of the initial deactivation during product gas run 1 (1100 h) and 2 (1400 h) along the first 24 h of operation.

the second run, the permeate flow of both runs are compared in Fig. 7 during the first 24 h of product gas exposure. During the observed timeframe both permeate flows are nearly halved. Furthermore deactivation progress for both runs is quite similar, which let us conclude that the partial deactivation does not impact the initial deactivation of the second run. 80% recovery of the effective membrane area, equivalent to the feed flow of 35 NmL min^{-1}, is enough to reproduce the deactivation data.

The hatched area in Fig. 6 indicates a period where a temperature variation was performed and is shown in detail in Fig. 8. After about 1720 h, the membrane temperature was increased in steps by 10 K from 300 °C to 340 °C. The permeate flow clearly increases with rising temperature. Since the transmembrane transport has most probably already reached a state, where it is completely limited by surface reactions due to an overall low number of available surface sites, the temperature should increase the adsorption equilibrium in favour of desorption of impurities making adsorption sites re-accessible for hydrogen.

For a quantitative analysis, the permeances at the respective temperature are shown in the Arrhenius plot in Fig. 9 and compared with the measurement at the beginning of the experiment (from Fig. 4) with an underlying Sieverts' exponent of 0.875. The activation energy for the hydrogen transmembrane transport is with 38 kJ mol^{-1}, when exposed to product gas (see Table 3), about threefold higher than when exposed to pure hydrogen and comparable to a 25 μm thick Pd-membrane at 170 °C [102]. In this case the determined activation energy is influenced by the desorption energy of contaminants. The pre-exponential factor, on the other hand, is about a factor of 10 higher than under pure hydrogen, which is clear due to the typical strong correlation between slope ($E_{A,M}$) and Q_0.

3.4. Long-term membrane regeneration with pure hydrogen

Regeneration of the membrane means cleaning of the surface by eventually hydrogenation of double bonds of the hydrocarbons and desorption of these compounds covering the active membrane surface. Also in our previous work [29] the degradation of the membrane under product gas for 8 h and its subsequent regeneration under pure hydrogen for 16 h by applying a reference point was examined. It could be shown that after 8 h the separation efficiency was reduced up to 30%, but as well that it could almost be completely restored [29]. As can be seen from the timeline in Fig. 3, the exposure to product gas in this work was extended in a first step to 24 h (section ②) with 11 days of regeneration (section ③) and subsequently even to 20 days (section ④) with 122 days

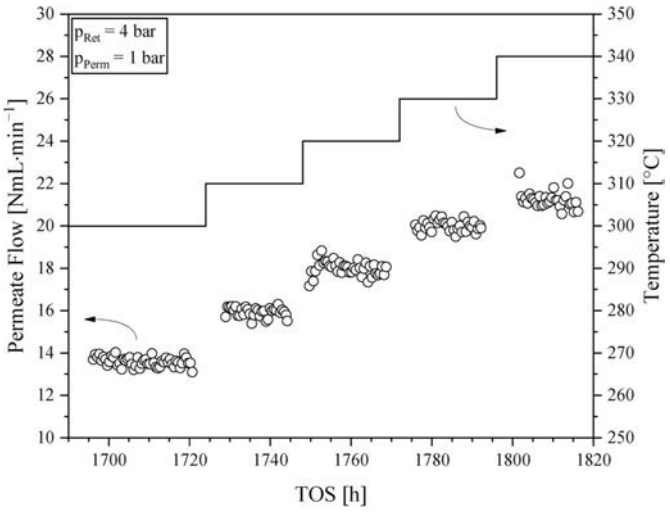

Fig. 8. Permeate flow as a function of time-on-stream during the stepwise increase of the temperature by 10 K/d from 300 °C to 340 °C under feed of product gas from dehydrogenation.

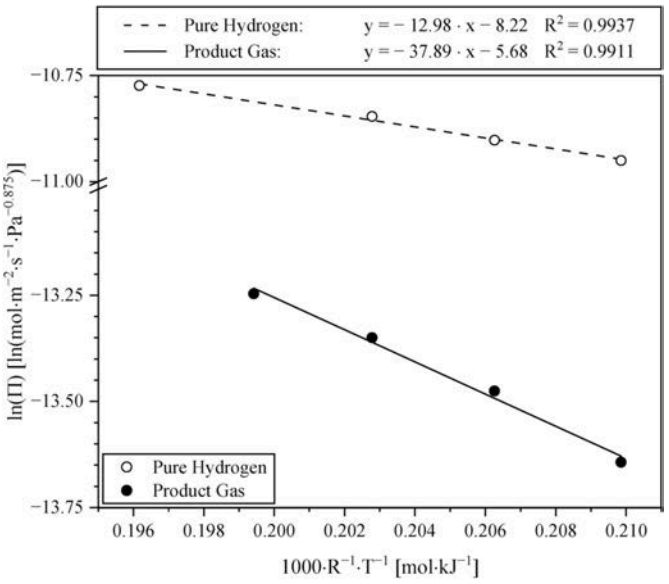

Fig. 9. Arrhenius plot of the measurements with pure hydrogen and with product gas from LOHC dehydrogenation in dependence of adjusted Sieverts' exponents of 0.875.

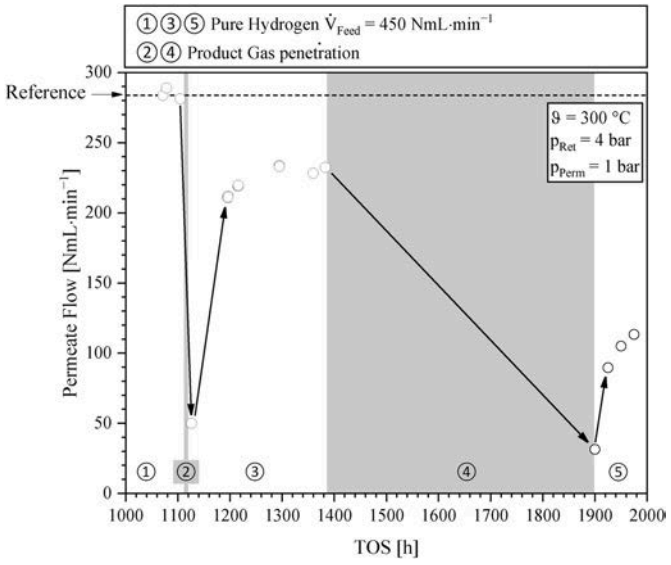

Fig. 10. Permeate flow referred to the reference flow of 283 NmL min^{-1} along the experiment duration of 2000 h. The gray areas (sections ② and ④) indicate the operating time with product gas.

of regeneration (section ⑤). The measured permeate flow at the reference point (feed flow of pure hydrogen at 450 NmL min^{-1} at 4 bar and 300 °C) is plotted over the TOS in Fig. 9 (for a better overview up to 2000 h TOS) and Fig. 11 (up to 5000 h TOS). The dotted line serves as a reference and indicates the measured permeate flow measured under pure hydrogen immediately before product gas was fed in for the first time.

With respect to the reference flow, it makes almost no difference whether the product gas is applied to the membrane for 24 h (– 83% at approx. 1100 h) or 480 h (– 88% at approx. 1900 h). This clearly shows that most of the degradation proceeds at the beginning and supports the hypothesis that the active membrane surface is quickly covered by the hydrocarbon molecules, which instantaneously inhibit the dissociative adsorption of hydrogen. As mentioned before, the low feed flow rate might have a large effect, which should be investigated in further

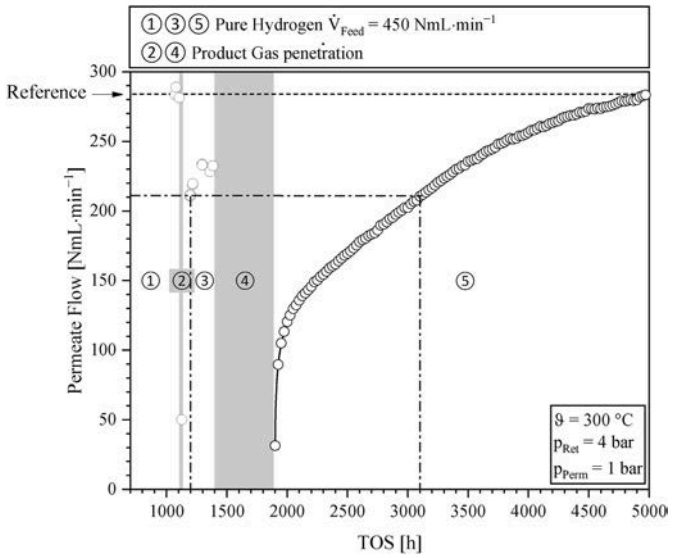

Fig. 11. Permeate flow referred to the reference flow of 283 NmL min ^{1} along the experiment duration of 5000 h. The gray areas (sections ② and ④) indicate the operating time with product gas.

Table 3
Evaluation of the activation energy and the pre-exponential factor from the temperature variation with pure hydrogen and product gas as a function of the adjusted Sieverts' exponent of 0.875.

Fit for n 0.875	$E_{A,M}$[kJ·mol ^{1}]	Q_0[mol·m ^{1}·Pa ^{n}·s ^{1}]
Pure hydrogen	12.98	2.69×10^{9}
Product gas	37.89	3.41×10^{8}

experiments.

The duration of product gas operation, however, has an enormous effect on the regeneration behaviour, which is clearly shown by comparing the permeate flows in section ③ and ⑤. With increasing operating time under product gas, the regeneration time increases. Following the dashed line drawn in Fig. 11 at 211 NmL min^{-1} (corresponding to 75% of the reference permeate flow), the regeneration time is extended by a factor of 17. Furthermore, it should be noted that the membrane could be regenerated completely with hydrogen, even if it took as long as 3000 h.

The extended regeneration time seems to be caused by the changed surface configuration of the deposited species with increasing exposure time to product gas. This fits to the conclusion provided by others: The amount of surface-adsorbed, sub-surface and bulk species increase sharply at beginning of the exposure. Sub-surface and bulk species are attributed to carbon atoms. The surface-adsorbed and sub-surface species reach a roughly constant value with increasing exposure time, while the amount of bulk species continue to grow. However, the influence on H_2-permeation is mainly associated with surface-adsorbed species [65].

Assuming that in our study mainly hydrocarbon molecules adsorb on the surface, it can be concluded that the hydrogenation of these components on Pd is accompanied by the formation of coke precursors or coke [55,103–106]. In experiments with propylene, the formation of components that are difficult to desorb under permanent load was suspected, while no PdC was found at 300 °C in Ref. [65]. Similar to degradation, the regeneration rate in Fig. 11 (section ⑤) is much higher at the beginning, which can be explained by desorption of weakly adsorbed components. The further gradual regeneration is caused by slow reaction of solid carbon or carbon precursors.

3.5. Permselectivity

Prior to the first exposure to the LOHC product gas (after 768 h) and after complete regeneration (after 4800 h) the permselectivity was measured and is shown in Table 4. After 768 h of hydrogen operation a value of 3144 was obtained, which is relatively low compared to previous studies [50], but not influencing the hydrogen flux at the applied pressure according to calculations.

Since a certain leakage of helium under vacuum was detected immediately after integrating the membrane in the microchannel assembly by laser welding (initial validation procedure during manufacture), the permselectivity (always performed with nitrogen) is lower from the beginning and should not have changed much during the initial 768 h. Although the operation of micro-structured Pd-membrane modules can result in the formation of pores, up to holes and cracks, due to the membrane deformation and the simultaneous increase in surface area during activation, the formation of cracks and holes is unlikely at the mild conditions currently applied (4 bar(a) and 300 °C).

During more than 4000 h of repeated product gas operation and subsequent regeneration, the permselectivity was nearly halved to a value of 1534. This decrease can usually be explained by the formation of pinholes due to the long operating time, which are caused by grain growth and intermetallic diffusion of silver and palladium [107]. Furthermore, the impact of adsorbed carbon is unknown. It has been reported that carbon can migrate from the surface of the membrane into the solid and cause an expansion of the PdAg-lattice [106]. During long term treatment with hydrogen, the carbon can also pass the material [106], leaving holes which increase the permeability for nitrogen.

For better understanding of these findings, the experiment was stopped after 5000 h of operation and pictures of the membrane surface and cross section were taken by scanning electron microscope (SEM). Note, that the membrane was fully intact when the experiment was stopped.

The cross section of the membrane module is presented in Fig. 12, where the hydrogen pathway is focused from the microchannel through a hole of the microsieve. The expected deformation of the membrane due to the pressure gradient between feed and permeate side can also be noticed. In comparison to Ref. [91], however, this deformation is significantly reduced. The reason for this is, on the one hand, the mild operating conditions of 300 °C and 4 bar(a), but also the different geometry, which minimizes the deformation and extends the lifetime. The micro holes are only 70–100 μm wide, while channels of 200 or 1000 μm width were used in Ref. [91]. Further, the hole geometry leads to less stress compared to a long channel. The higher membrane thickness in the uncovered area compared to the covered area is against the expectation. A lower thickness would be result of bending; however, as preparation of the embedded cross section, lattice-hydrogen and enrichment of steel components are excluded, the reason for the thicker membrane below the micro holes remains unclear. Hydrogen was swept out by nitrogen at the end of the experiment and steel components have not been found in elemental analysis. The thicker region is not a singularity, but has been detected in all holes.

Elemental analysis (EDX, energy dispersive X-ray spectroscopy) in Fig. 13 was performed in the middle of the uncovered cross-sectional area of the membrane. Fig. 13 (b) shows a clear segregation of Pd towards the feed surface of the membrane in the direction of the feed side, while Ag-atoms accumulate in the bulk (see Fig. 13 (b)). This segregation is explained by the strong binding energy of palladium and

Table 4
Comparison of permselectivity before product gas operation (after 768 h) and after complete regeneration.

	Permselectivity [−]
Before product gas operation (TOS 768 h)	3144 ± 13
After completed regeneration (TOS 4800 h)	1534 ± 15

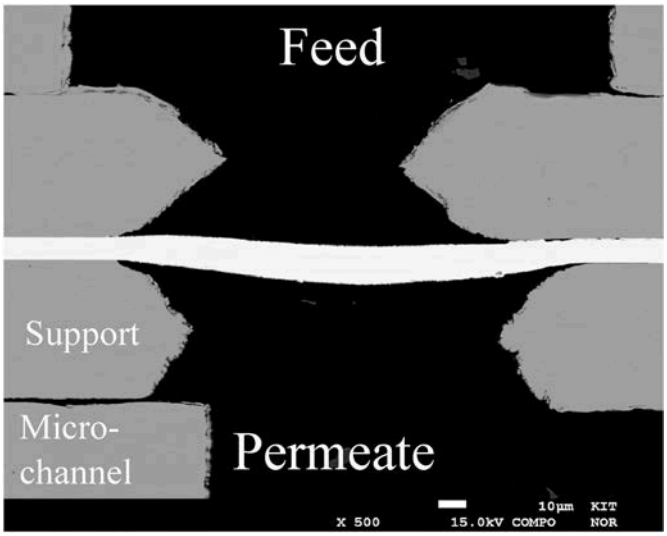

Fig. 12. Cross section of the membrane module with uncovered and supported section of the membrane.

hydrogen, which causes an energetic imbalance between surface on the feed site and bulk regarding the PdAg-distribution [108–110]. Since Pd is isolated in some part the benefit of the added Ag is not given anymore, as the suppressed phase transition can occur. An elemental analysis of carbon was also carried out (not shown), where carbon was detected on both surfaces of the membrane. However, the presence of carbon is mainly caused by the embedding material used to prepare the sample. A clear statement regarding the possible carbon deposits originating from the experiment can therefore not be made. Interestingly, both Ag and Pd signals are lower in a region of about 2 µm at the permeate side. No other material has been detected in this region. Thus, the density of Pd + Ag is different and might be an explanation of the thicker membrane under the holes of the micro sieve. The separation effect on permeate side and the lower "PdAg density" has not been detected in the covered region of the membrane. In analogy to Fig. 13 corresponding SEM-image and elemental mappings were applied for a region where the membrane were covered by the metal support (see Fig. 14). Fig. 14 (b) and (c) clearly do not show such kind of strong segregation – these maps are close to the original membrane before exposure. The covered area is much less accessible for hydrogen permeation, so that the hydrogen and/or product gas penetration and permeation seems responsible for the segregation. Although such severe segregation is not expected at the applied conditions and is never reported in literature, the long-term operation seems to promote changes within the membrane structure.

Images of the surface on the feed and permeate side in the uncovered area of the membrane are shown in Fig. 15. Comparing the feed and permeate side, it can be noticed that the grains are larger on the feed side as on the permeate side. However, this finding is not a result of a stronger grain growth on the feed side, but rather caused by the manufacturing process. When sputtering onto a substrate, the grain size increases with increasing thickness [111]. Therefore, the permeate side corresponds to side facing the substrate during sputtering. Contrary to previous investigations of microchannel-integrated thin films [91], neither cracks nor holes are apparent on the surface. The surface of the feed side was examined at more than ten different locations with the same result. The reason is the low operating temperature of 300 °C and the low operating pressure of 3 bar(a) in addition to the good supporting properties of the applied microsieves that have much smaller dimensions compared to the 200 and 1000 µm channels applied in Ref. [91], which barely change the surface morphology. As expected after a long regeneration with hydrogen, no carbon deposits have been found.

In summary, the decrease in permselectivity is not the result of changes in membrane properties due to temperature, pressure, or contamination, but rather to the possible growth of existing leaks points originated from the laser welding. Under the applied operating conditions, the life estimation of 2–7 years is realistic [107,112].

4. Conclusion

For the application of hydrogen in fuel cell vehicles from LOHC dehydrogenation, the post-treatment of the hydrogen is necessary since the required limits of carbon monoxide and hydrocarbons cannot be met. The purification of the product gas using PdAg-membranes is promising, since the membrane can be combined well with the operating conditions of the dehydrogenation. However, the impurities present in the product gas can reduce the performance of the membrane. Therefore, in this work we performed investigations at 300 °C and 4 bars for long-term degradation under product gas, regeneration under pure hydrogen and long-term stability.

The impurities present in the product gas can cause an instantaneous strong decrease in hydrogen flux, subsequently the hydrogen flux is further declining at a constant rate. The initial strong decrease is not attributed to extreme concentration of impurities since the reactor and membrane coupling almost immediately leads to 25% retentate flow. Two different degradation mechanisms are assumed to be involved in this transition: the adsorption of hydrocarbon molecules (excluding methane) in the product gas stream and the formation of coke-precursors or even coke on the membrane surface over time. The longer the membrane is operated with product gas, the longer the membrane needs to be regenerated. The hydrogen flux has been completely restored by treatment with pure hydrogen.

After the integration of the membrane in the module by laser welding, an initial leakage was detected which resulted in a relatively low permselectivity of about 3100 in the time of membrane activation under hydrogen. Since such initial leakage occurs from time to time in the manufacturing process, the process of module welding must be improved to be more reproducible in the future. The reduction in permselectivity by 50% over an operating time of 4000 h is not related to an ageing phenomena of palladium membranes. Post-images show that the mechanical deformation of the membrane under pressure is not very distinct and neither holes nor pores are visible. Furthermore, no influence of the contaminants on the morphology of the membrane on feed side could be observed. The decrease in permselectivity is therefore only caused by the enlargement of the existing leaks that occurred during laser welding. These findings prove that the concept with the micro sieve used as membrane support has a high stability far beyond the investigated period of approx. 5000 h. In combination with the relatively mild conditions of 300 °C and 4 bar(a), the membrane lifetime can be estimated to many years.

The permeation process in presence of the LOHC contaminants is limited by adsorptive dissociation of hydrogen on the membrane surface, which becomes critical after longer exposure times. The impurities result in a three-fold increase of the activation energy (38 kJ mol^{-1}) compared to pure hydrogen. Although the original separation efficiency could be restored by flushing with pure hydrogen, the technical implementation of flushing with pure hydrogen is not practical given the rapid degradation and slow regeneration. In the next step, the pre- and post-treatment of the membrane with air or oxygen is planned in order to (re)activate the membrane faster. The installation of activated carbon filters for pre-cleaning the product gas is also planned to remove the hydrocarbon contaminants from the gas stream.

Author contributions

Conceptualization, A.W., E.G. and P.P.; methodology, A.W. and E.G.; software, A.W. and E.G.; validation, A.W., E.G. and P.P.; formal analysis, A.W., E.G. and P.P.; investigation, A.W. and E.G.; resources, A.W. and E. G.; data curation, A.W. and E.G.; writing—original draft preparation, A.

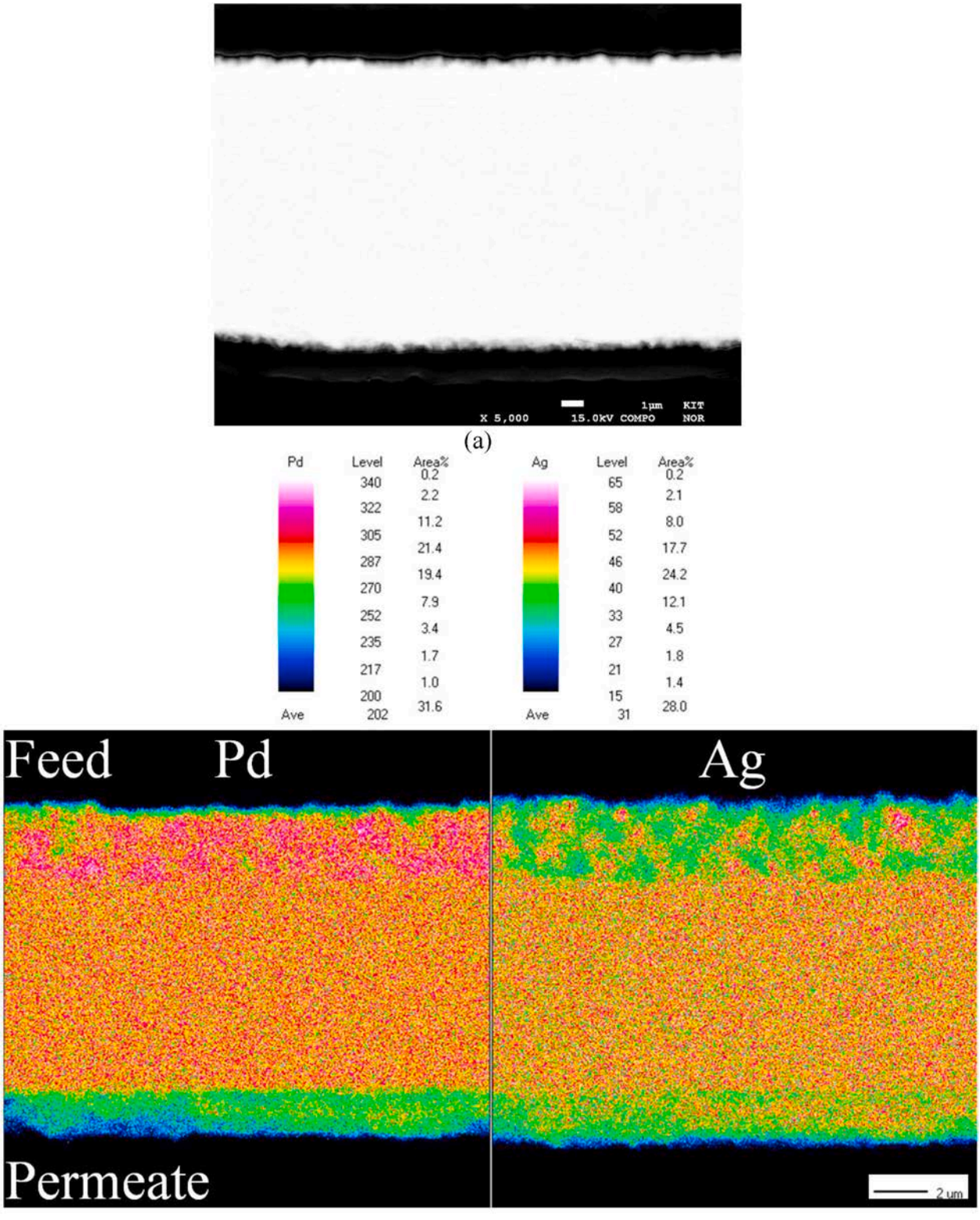

Fig. 13. Elemental mapping by energy dispersive X-ray spectroscopy of the **uncovered** section of the membrane illustrated in Fig. 12: (a) SEM-Image (b) palladium; (c) silver. The colours/level in the bar represent the signal of the component relative to the highest signal detected in this sample. The provided area% is not a concentration but the picture area which is covered from the colour/level in relation to the overall picture area. (For interpretation of the references to colour in this figure legend, the reader is referred to the Web version of this article.)

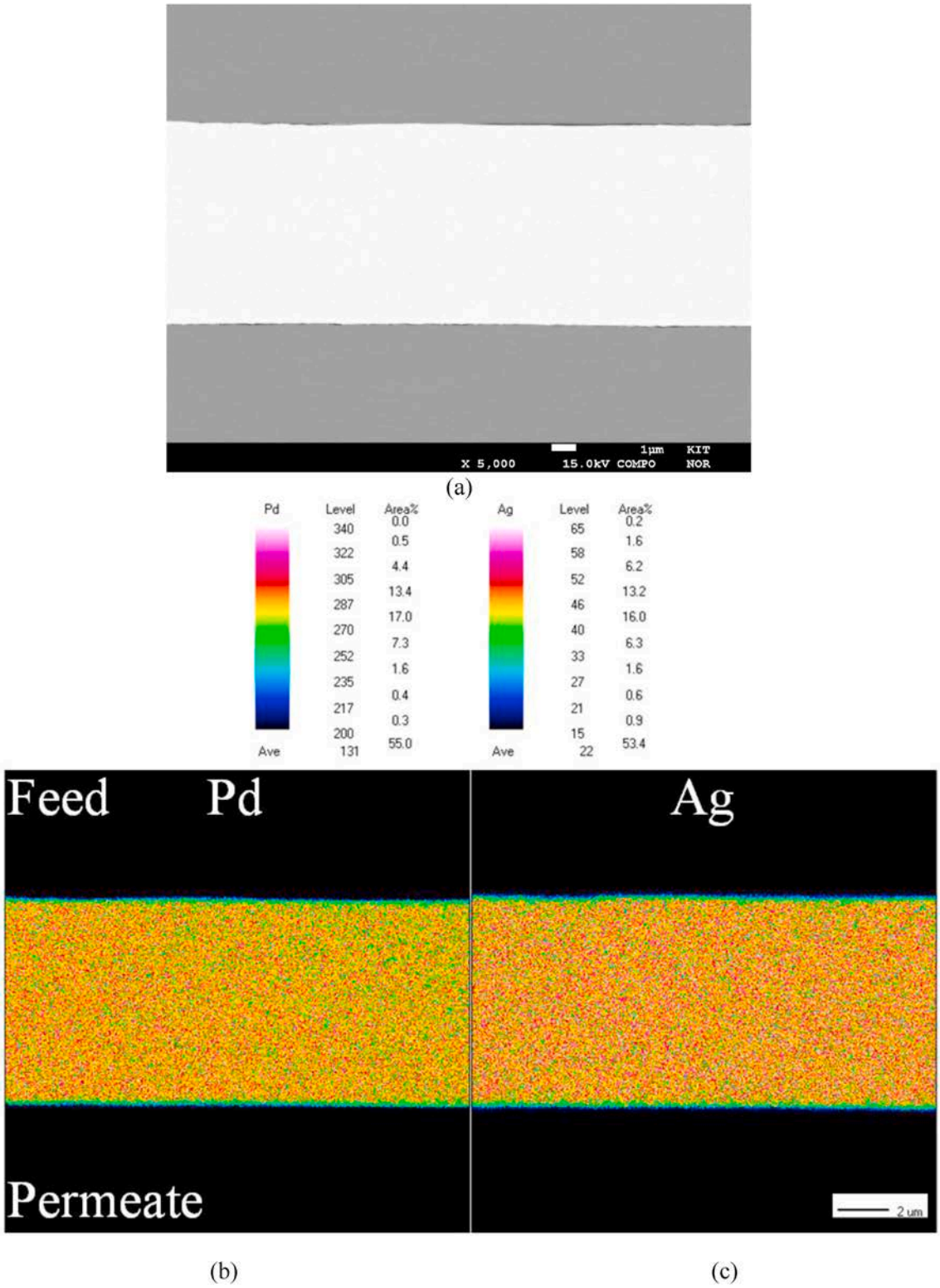

Fig. 14. Elemental mapping by energy dispersive X-ray spectroscopy of the **covered** section of the membrane illustrated in Fig. 12: (a) SEM-Image (b) palladium; (c) silver. The colours/level in the bar represent the signal of the component relative to the highest signal detected in this sample. The provided area% is not a concentration but the picture area which is covered from the colour/level in relation to the overall picture area. (For interpretation of the references to colour in this figure legend, the reader is referred to the Web version of this article.)

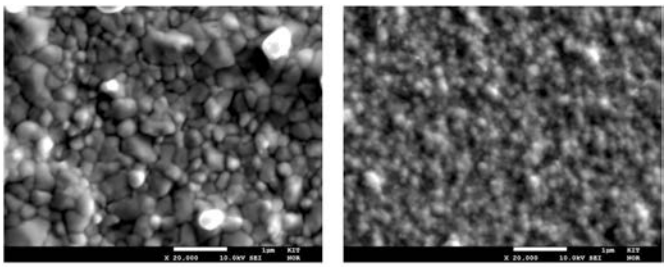

Fig. 15. SEM-pictures of the PdAg-membrane after 5000 h of operation: (a) feed side; (b) permeate side.

W.; writing—review and editing, E.G., T.P. and P.P.; visualization, A.W. and E.G.; supervision, P.P.; project administration, P.P.; funding acquisition, P.P. All authors have read and agreed to the published version of the manuscript.

Funding

The authors gratefully acknowledge funding by the German Federal Ministry of Education and Research (BMBF) within the Kopernikus Project P2X: Flexible use of renewable resources—exploration, validation, and implementation of 'Power-to-X' concepts (contract no. 03SFK2K0 and 03SFK2K0-2).

Declaration of competing interest

The authors declare that they have no known competing financial interests or personal relationships that could have appeared to influence the work reported in this paper.

Acknowledgments

The author thanks Uta Gerhards from KIT-IMVT for SEM-analysis of the membrane, and Marit Stange from SINTEF for the manufacturing of the PdAg-foils.

References

[1] S. Droge, Das Pariser Abkommen 2015: weichenstellung für das Klimaregime, in: Stiftung Wissenschaft und Politik -SWP- Deutsches Institut für Internationale Politik und Sicherheit, 19/2015, 2015, p. 34.
[2] Bundesministerium für Umwelt Naturschutz und nukleare Sicherheit (BMU), Klimaschutzplan 2050 - Klimaschutzpolitische Grundsatze und Ziele der Bundesregierung, 2016.
[3] J. Chabot, J. Lecomte, C. Grumet, J. Sannier, Fuel clean-up system: poisoning of palladium-silver membranes by gaseous impurities, Fusion Technol. 14 (2P2A) (1988) 614–618, https://doi.org/10.13182/fst88-a25202.
[4] M. Momirlan, T.N. Veziroglu, The properties of hydrogen as fuel tomorrow in sustainable energy system for a cleaner planet, Int. J. Hydrogen Energy 30 (7) (2005) 795–802, https://doi.org/10.1016/j.ijhydene.2004.10.011.
[5] P.T. Aakko-Saksa, C. Cook, J. Kiviaho, T. Repo, Liquid organic hydrogen carriers for transportation and storing of renewable energy – review and discussion, J. Power Sources 396 (2018) 803–823, https://doi.org/10.1016/j.jpowsour.2018.04.011.
[6] C. Lang, Y. Jia, X. Yao, Recent advances in liquid-phase chemical hydrogen storage, Energy Storage Mater. 26 (2020) 290–312, https://doi.org/10.1016/j.ensm.2020.01.010.
[7] P. Preuster, A. Alekseev, P. Wasserscheid, Hydrogen storage technologies for future energy systems, Annu. Rev. Chem. Biomol. Eng. 8 (1) (2017) 445–471, https://doi.org/10.1146/annurev-chembioeng-060816-101334.
[8] P.M. Modisha, C.N.M. Ouma, R. Garidzirai, P. Wasserscheid, D. Bessarabov, The prospect of hydrogen storage using liquid organic hydrogen carriers, Energy Fuel. 33 (4) (2019) 2778–2796, https://doi.org/10.1021/acs.energyfuels.9b00296.
[9] M. Markiewicz, Y.-Q. Zhang, M.T. Empl, M. Lykaki, J. Thoming, P. Steinberg, S. Stolte, Hazard assessment of quinaldine-, alkylcarbazole-, benzene- and toluene-based liquid organic hydrogen carrier (LOHCs) systems, Energy Environ. Sci. 12 (1) (2019) 366–383, https://doi.org/10.1039/c8ee01696h.
[10] M. Markiewicz, Y.Q. Zhang, A. Bosmann, N. Bruckner, J. Thoming, P. Wasserscheid, S. Stolte, Environmental and health impact assessment of Liquid Organic Hydrogen Carrier (LOHC) systems - challenges and preliminary results, Energy Environ. Sci. 8 (3) (2015) 1035–1045, https://doi.org/10.1039/c4ee03528c.
[11] K. Müller, J. Volkl, W. Arlt, Thermodynamic evaluation of potential organic hydrogen carriers, Energy Technol. 1 (1) (2013) 20–24, https://doi.org/10.1002/ente.201200045.
[12] N. Bruckner, K. Obesser, A. Bosmann, D. Teichmann, W. Arlt, J. Dungs, P. Wasserscheid, Evaluation of industrially applied heat-transfer fluids as liquid organic hydrogen carrier systems, ChemSusChem 7 (1) (2014) 229–235, https://doi.org/10.1002/cssc.201300426.
[13] D. Teichmann, W. Arlt, P. Wasserscheid, Liquid Organic Hydrogen Carriers as an efficient vector for the transport and storage of renewable energy, Int. J. Hydrogen Energy 37 (23) (2012) 18118–18132, https://doi.org/10.1016/j.ijhydene.2012.08.066.
[14] D. Teichmann, K. Stark, K. Muller, G. Zottl, P. Wasserscheid, W. Arlt, Energy storage in residential and commercial buildings via liquid organic hydrogen carriers (LOHC), Energy Environ. Sci. 5 (10) (2012) 9044–9054, https://doi.org/10.1039/c2ee22070a.
[15] M. Reuß, T. Grube, M. Robinius, P. Preuster, P. Wasserscheid, D. Stolten, Seasonal storage and alternative carriers: a flexible hydrogen supply chain model, Appl. Energy 200 (2017) 290–302, https://doi.org/10.1016/j.apenergy.2017.05.050.
[16] M. Reuß, T. Grube, M. Robinius, D. Stolten, A hydrogen supply chain with spatial resolution: comparative analysis of infrastructure technologies in Germany, Appl. Energy 247 (2019) 438–453, https://doi.org/10.1016/j.apenergy.2019.04.064.
[17] A. Haupt, K. Muller, Integration of a LOHC storage into a heat-controlled CHP system, Energy 118 (2017) 1123–1130, https://doi.org/10.1016/j.energy.2016.10.129.
[18] C. Krieger, K. Muller, W. Arlt, Coupling of a liquid organic hydrogen carrier system with industrial heat, Chem. Eng. Technol. 39 (8) (2016) 1570–1574, https://doi.org/10.1002/ceat.201600180.
[19] N. El-Taweel, H. Khani, H.E.Z. Farag, Optimal sizing and scheduling of LOHC-based generation and storage plants for concurrent services to transportation sector and ancillary services market, IEEE Trans. Sustain. Energy (2019), https://doi.org/10.1109/TSTE.2019.2926456, 1-1.
[20] V. Oldenbroek, G. Smink, T. Salet, A.J.M. van Wijk, Fuel cell electric vehicle as a power plant: techno-economic scenario analysis of a renewable integrated transportation and energy system for smart cities in two climates, Appl. Sci. 10 (1) (2019) 143.
[21] M. Eypasch, M. Schimpe, A. Kanwar, T. Hartmann, S. Herzog, T. Frank, T. Hamacher, Model-based techno-economic evaluation of an electricity storage system based on Liquid Organic Hydrogen Carriers, Appl. Energy 185 (2017) 320–330, https://doi.org/10.1016/j.apenergy.2016.10.068.
[22] M. Niermann, S. Drünert, M. Kaltschmitt, K. Bonhoff, Liquid organic hydrogen carriers (LOHCs) – techno-economic analysis of LOHCs in a defined process chain, Energy Environ. Sci. 12 (1) (2019) 290–307, https://doi.org/10.1039/c8ee02700e.
[23] M. Hurskainen, Liquid Organic Hydrogen Carriers (LOHC): Concept Evaluation and Techno-Economics, VTT Technical Research Centre of Finland, 2019. Research Report, No. VTT-R-00057-19.
[24] W. Arlt, J. Obermeier, Machbarkeitsstudie - Wasserstoff und Speicherung im Schwerlastverkehr, Institut für Thermische Verfahrenstechnik, Universitat Nürnberg-Erlangen, 2017.
[25] C. Hank, A. Sternberg, N. Koppel, M. Holst, T. Smolinka, A. Schaadt, H.-M. Henning, Energy efficiency and economic assessment of imported energy carriers based on renewable electricity, Sustain. Energy Fuels (2020), https://doi.org/10.1039/D0SE00067A.
[26] C. Wulf, M. Reuß, T. Grube, P. Zapp, M. Robinius, J.-F. Hake, D. Stolten, Life Cycle Assessment of hydrogen transport and distribution options, J. Clean. Prod. 199 (2018) 431–443, https://doi.org/10.1016/j.jclepro.2018.07.180.
[27] A. Seidel, Refuelling of fuel cell vehicles by hydrogen from the LOHC process gas for energy, 2019, pp. 2–8, 1/2019.
[28] T. Luschtinetz, A. Sklarow, J. Gulden, Degradation effects on PEM fuel cells supplied with hydrogen from a LOHC system, Appl. Mech. Mater. 839 (2016) 165–169. https://doi.org/10.4028/www.scientific.net/AMM.839.165.
[29] A. Wunsch, T. Berg, P. Pfeifer, Hydrogen production from the LOHC perhydro-dibenzyl-toluene and purification using a 5 μm PdAg-membrane in a coupled microstructured system, Materials 13 (2) (2020) 277, https://doi.org/10.3390/ma13020277.
[30] H. Jorschick, S. Dürr, P. Preuster, A. Bosmann, P. Wasserscheid, Operational stability of a LOHC-based hot pressure swing reactor for hydrogen storage, Energy Technol. 7 (1) (2018) 146–152, https://doi.org/10.1002/ente.201800499.
[31] H. Jorschick, P. Preuster, S. Durr, A. Seidel, K. Muller, A. Bosmann, P. Wasserscheid, Hydrogen storage using a hot pressure swing reactor, Energy Environ. Sci. 10 (7) (2017) 1652–1659, https://doi.org/10.1039/c7ee00476a.
[32] A. Bulgarin, H. Jorschick, P. Preuster, A. Bosmann, P. Wasserscheid, Purity of hydrogen released from the Liquid Organic Hydrogen Carrier compound perhydro dibenzyltoluene by catalytic dehydrogenation, Int. J. Hydrogen Energy 45 (1) (2020) 712–720, https://doi.org/10.1016/j.ijhydene.2019.10.067.
[33] A. Wunsch, M. Mohr, P. Pfeifer, Intensified LOHC-dehydrogenation using multi-stage microstructures and Pd-based membranes, Membranes 8 (4) (2018) 112, https://doi.org/10.3390/membranes8040112.
[34] S.N. Paglieri, J.D. Way, Innovations in palladium membrane Research, Separ. Purif. Methods 31 (1) (2002) 1–169, https://doi.org/10.1081/SPM-120006115.
[35] A. Basile, A. Iulianelli, T. Longo, S. Liguori, M. De Falco, Pd-based selective membrane state-of-the-art, in: M. De De Falco, L. Marrelli, G. Iaquaniello (Eds.),

Membrane Reactors for Hydrogen Production Processes, Springer London, London, 2011, pp. 21–55.
[36] L. Marrelli, M. De Falco, G. Iaquaniello, Integration of selective membranes in chemical processes: benefits and examples, in: M. De De Falco, L. Marrelli, G. Iaquaniello (Eds.), Membrane Reactors for Hydrogen Production Processes, Springer London, London, 2011, pp. 1–19.
[37] J.J. Conde, M. Marono, J.M. Sánchez-Hervás, Pd-based membranes for hydrogen separation: review of alloying elements and their influence on membrane properties, Separ. Purif. Rev. 46 (2) (2016) 152–177, https://doi.org/10.1080/15422119.2016.1212379.
[38] G.L. Holleck, Diffusion and solubility of hydrogen in palladium and palladium–silver alloys, J. Phys. Chem. 74 (3) (1970) 503–511, https://doi.org/10.1021/j100698a005.
[39] B. Horst, P. Eva, Wasserstoff in palladium/silber-legierungen, Z. Phys. Chem. 44 (3_4) (1965) 143–159, https://doi.org/10.1524/zpch.1965.44.3_4.143.
[40] C.G. Sonwane, J. Wilcox, Y.H. Ma, Achieving optimum hydrogen permeability in PdAg and PdAu alloys, J. Chem. Phys. 125 (18) (2006) 184714, https://doi.org/10.1063/1.2387166.
[41] S. Uemiya, T. Matsuda, E. Kikuchi, Hydrogen permeable palladium-silver alloy membrane supported on porous ceramics, J. Membr. Sci. 56 (3) (1991) 315–325, https://doi.org/10.1016/S0376-7388(00)83041-0.
[42] H. Yoshida, K. Okuno, Y. Naruse, T. Kashiwai, Metallurgical considerations on Pd, Pd-alloy and their metal-hydrogen systems, Fusion Technol. 8 (2P2) (1985) 2388–2394, https://doi.org/10.13182/FST85-A24636.
[43] A. Caravella, G. Barbieri, E. Drioli, Concentration polarization analysis in self-supported Pd-based membranes, Separ. Purif. Technol. 66 (3) (2009) 613–624, https://doi.org/10.1016/j.seppur.2009.01.008.
[44] A. Caravella, Y. Sun, Correct evaluation of the effective concentration polarization influence in membrane-assisted devices. Case study: H2 production by Water Gas Shift in Pd-membrane reactors, Int. J. Hydrogen Energy 41 (27) (2016) 11653–11659, https://doi.org/10.1016/j.ijhydene.2015.12.068.
[45] J. Catalano, M. Giacinti Baschetti, G.C. Sarti, Influence of the gas phase resistance on hydrogen flux through thin palladium–silver membranes, J. Membr. Sci. 339 (1) (2009) 57–67, https://doi.org/10.1016/j.memsci.2009.04.032.
[46] W.-H. Chen, M.-H. Hsia, Y.-H. Chi, Y.-L. Lin, C.-C. Yang, Polarization phenomena of hydrogen-rich gas in high-permeance Pd and Pd–Cu membrane tubes, Appl. Energy 113 (2014) 41–50, https://doi.org/10.1016/j.apenergy.2013.07.014.
[47] W.-H. Chen, W.-Z. Syu, C.-I. Hung, Numerical characterization on concentration polarization of hydrogen permeation in a Pd-based membrane tube, Int. J. Hydrogen Energy 36 (22) (2011) 14734–14744, https://doi.org/10.1016/j.ijhydene.2011.08.043.
[48] S. Hara, K. Sakaki, N. Itoh, Decline in hydrogen permeation due to concentration polarization and CO hindrance in a palladium membrane reactor, Ind. Eng. Chem. Res. 38 (12) (1999) 4913–4918, https://doi.org/10.1021/ie990200n.
[49] F. Gallucci, F. Chiaravalloti, S. Tosti, E. Drioli, A. Basile, The effect of mixture gas on hydrogen permeation through a palladium membrane: experimental study and theoretical approach, Int. J. Hydrogen Energy 32 (12) (2007) 1837–1845, https://doi.org/10.1016/j.ijhydene.2006.09.034.
[50] T. Boltken, M. Belimov, P. Pfeifer, T.A. Peters, R. Bredesen, R. Dittmeyer, Fabrication and testing of a planar microstructured concept module with integrated palladium membranes, Chem. Eng. Process 67 (2013) 136–147, https://doi.org/10.1016/j.cep.2012.06.009.
[51] T.L. Ward, T. Dao, Model of hydrogen permeation behavior in palladium membranes, J. Membr. Sci. 153 (2) (1999) 211–231, https://doi.org/10.1016/S0376-7388(98)00256-7.
[52] S. Yun, S. Ted Oyama, Correlations in palladium membranes for hydrogen separation: a review, J. Membr. Sci. 375 (1) (2011) 28–45, https://doi.org/10.1016/j.memsci.2011.03.057.
[53] M. Coroneo, G. Montante, J. Catalano, A. Paglianti, Modelling the effect of operating conditions on hydrodynamics and mass transfer in a Pd–Ag membrane module for H2 purification, J. Membr. Sci. 343 (1) (2009) 34–41, https://doi.org/10.1016/j.memsci.2009.07.008.
[54] K. Hou, R. Hughes, The effect of external mass transfer, competitive adsorption and coking on hydrogen permeation through thin Pd/Ag membranes, J. Membr. Sci. 206 (1–2) (2002) 119–130, https://doi.org/10.1016/S0376-7388(01)00770-0.
[55] H. Li, A. Goldbach, W. Li, H. Xu, PdC formation in ultra-thin Pd membranes during separation of H2/CO mixtures, J. Membr. Sci. 299 (1–2) (2007) 130–137, https://doi.org/10.1016/j.memsci.2007.04.034.
[56] A.B. Antoniazzi, A.A. Haasz, P.C. Stangeby, The effect of adsorbed carbon and sulphur on hydrogen permeation through palladium, J. Nucl. Mater. 162–164 (1989) 1065–1070, https://doi.org/10.1016/0022-3115(89)90410-8.
[57] M. Eriksson, L.G. Ekedahl, Real time measurements of hydrogen desorption and absorption during CO exposures of Pd: hydrogen sticking and dissolution, Appl. Surf. Sci. 133 (1) (1998) 89–97, https://doi.org/10.1016/S0169-4332(98)00185-8.
[58] H. Amandusson, L.G. Ekedahl, H. Dannetun, The effect of CO and O2 on hydrogen permeation through a palladium membrane, Appl. Surf. Sci. 153 (4) (2000) 259–267, https://doi.org/10.1016/S0169-4332(99)00357-8.
[59] Y. Ma, J. Bansmann, T. Diemant, R.J. Behm, Formation, stability and CO adsorption properties of PdAg/Pd(111) surface alloys, Surf. Sci. 603 (7) (2009) 1046–1054, https://doi.org/10.1016/j.susc.2009.02.024.
[60] A.L. Mejdell, D. Chen, T.A. Peters, R. Bredesen, H.J. Venvik, The effect of heat treatment in air on CO inhibition of a ~3μm Pd–Ag (23wt.%) membrane, J. Membr. Sci. 350 (1) (2010) 371–377, https://doi.org/10.1016/j.memsci.2010.01.012.
[61] A.L. Mejdell, M. Jøndahl, T.A. Peters, R. Bredesen, H.J. Venvik, Effects of CO and CO2 on hydrogen permeation through a ~3μm Pd/Ag 23wt.% membrane employed in a microchannel membrane configuration, Separ. Purif. Technol. 68 (2) (2009) 178–184, https://doi.org/10.1016/j.seppur.2009.04.025.
[62] C.V. Miguel, A. Mendes, S. Tosti, L.M. Madeira, Effect of CO and CO2 on H2 permeation through finger-like Pd–Ag membranes, Int. J. Hydrogen Energy 37 (17) (2012) 12680–12687, https://doi.org/10.1016/j.ijhydene.2012.05.131.
[63] C.P. O'Brien, I.C. Lee, CO poisoning and CO hydrogenation on the surface of Pd hydrogen separation membranes, J. Phys. Chem. C 121 (31) (2017) 16864–16871, https://doi.org/10.1021/acs.jpcc.7b05046.
[64] C.P. O'Brien, Z.W. Dunbar, I.C. Lee, A spectroscopic membrane permeation cell for in-situ infrared-reflection absorption spectroscopic analysis of membrane surfaces and simultaneous measurement of trans-membrane gas permeation rates, J. Membr. Sci. 526 (2017) 43–51, https://doi.org/10.1016/j.memsci.2016.12.016.
[65] J. Easa, R. Jin, C.P. O'Brien, Evolution of surface and bulk carbon species derived from propylene and their influence on the interaction of hydrogen with palladium, J. Membr. Sci. 596 (2020), https://doi.org/10.1016/j.memsci.2019.117738.
[66] V.V. Kaichev, M. Morkel, H. Unterhalt, I.P. Prosvirin, V.I. Bukhtiyarov, G. Rupprechter, H.J. Freund, C–O bond scission on "defect-rich and perfect" Pd (111)? Surf. Sci. 566–568 (2004) 1024–1029, https://doi.org/10.1016/j.susc.2004.06.100.
[67] V. Matolin, M. Rebholz, N. Kruse, Defect-induced dissociation of CO on palladium, Surf. Sci. 245 (3) (1991) 233–243, https://doi.org/10.1016/0039-6028(91)90026-O.
[68] I.-H. Svenum, J.A. Herron, M. Mavrikakis, H.J. Venvik, Pd3Ag(111) as a model system for hydrogen separation membranes: combined effects of CO adsorption and surface termination on the activation of molecular hydrogen, Top. Catal. (2020), https://doi.org/10.1007/s11244-020-01246-7.
[69] Z.W. Dunbar, I.C. Lee, Effects of elevated temperatures and contaminated hydrogen gas mixtures on novel ultrathin palladium composite membranes, Int. J. Hydrogen Energy 42 (49) (2017) 29310–29319, https://doi.org/10.1016/j.ijhydene.2017.10.032.
[70] F.C. Gielens, R.J.J. Knibbeler, P.F.J. Duysinx, H.D. Tong, M.A.G. Vorstman, J.T. F. Keurentjes, Influence of steam and carbon dioxide on the hydrogen flux through thin Pd/Ag and Pd membranes, J. Membr. Sci. 279 (1) (2006) 176–185, https://doi.org/10.1016/j.memsci.2005.12.002.
[71] F. Chen, Y. Kinari, F. Sakamoto, Y. Nakayama, Y. Sakamoto, Hydrogen permeation through palladium-based alloy membranes in mixtures of 10% methane and ethylene in the hydrogen, Int. J. Hydrogen Energy 21 (7) (1996) 555–561, https://doi.org/10.1016/0360-3199(95)00119-0.
[72] R.G. Musket, Effects of contamination on the interaction of hydrogen gas with palladium: a review, J. Less Common Met. 45 (2) (1976) 173–183, https://doi.org/10.1016/0022-5088(76)90265-4.
[73] S.H. Jung, K. Kusakabe, S. Morooka, S.-D. Kim, Effects of co-existing hydrocarbons on hydrogen permeation through a palladium membrane, J. Membr. Sci. 170 (1) (2000) 53–60, https://doi.org/10.1016/S0376-7388(99)00357-9.
[74] T.A. Peters, O. Liron, R. Tschentscher, M. Sheintuch, R. Bredesen, Investigation of Pd-based membranes in propane dehydrogenation (PDH) processes, Chem. Eng. J. 305 (2015) 191–200, https://doi.org/10.1016/j.cej.2015.09.068.
[75] K. Sato, T.-a. Hanaoka, S.-i. Niwa, C. Stefan, T. Namba, F. Mizukami, Direct hydroxylation of aromatic compounds by a palladium membrane reactor, Catal. Today 104 (2) (2005) 260–266, https://doi.org/10.1016/j.cattod.2005.03.067.
[76] H. Montesinos, I. Julián, J. Herguido, M. Menéndez, Effect of the presence of light hydrocarbon mixtures on hydrogen permeance through Pd–Ag alloyed membranes, Int. J. Hydrogen Energy 40 (8) (2015) 3462–3471, https://doi.org/10.1016/j.ijhydene.2014.11.054.
[77] S.-i. Niwa, M. Eswaramoorthy, J. Nair, A. Raj, N. Itoh, H. Shoji, F. Mizukami, A one-step conversion of benzene to phenol with a palladium membrane, Science 295 (5552) (2002) 105–107, https://doi.org/10.1126/science.1066527.
[78] S. Uemiya, I. Koike, E. Kikuchi, Promotion of the conversion of propane to aromatics by use of a palladium membrane, Appl. Catal. 76 (2) (1991) 171–181, https://doi.org/10.1016/0166-9834(91)80045-X.
[79] L. Bortolotto, R. Dittmeyer, Direct hydroxylation of benzene to phenol in a novel microstructured membrane reactor with distributed dosing of hydrogen and oxygen, Separ. Purif. Technol. 73 (1) (2010) 51–58, https://doi.org/10.1016/j.seppur.2009.10.019.
[80] M. Cholewa, B. Zehner, H. Kreuder, P. Pfeifer, Optimization of membrane area to catalyst mass in a microstructured membrane reactor for dehydrogenation of methylcyclohexane, Chem. Eng. Process 125 (2018) 325–333, https://doi.org/10.1016/j.cep.2017.10.011.
[81] H. Kreuder, T. Boeltken, M. Cholewa, J. Meier, P. Pfeifer, R. Dittmeyer, Heat storage by the dehydrogenation of methylcyclohexane - experimental studies for the design of a microstructured membrane reactor, Int. J. Hydrogen Energy 41 (28) (2016) 12082–12092, https://doi.org/10.1016/j.ijhydene.2016.05.140.
[82] H. Kreuder, C. Muller, J. Meier, U. Gerhards, R. Dittmeyer, P. Pfeifer, Catalyst development for the dehydrogenation of MCH in a microstructured membrane reactor-For heat storage by a Liquid Organic Reaction Cycle, Catal. Today 242 (2015) 211–220, https://doi.org/10.1016/j.cattod.2014.06.029.
[83] R. Dittmeyer, V. Hollein, K. Daub, Membrane reactors for hydrogenation and dehydrogenation processes based on supported palladium, J. Mol. Catal. Chem. 173 (1–2) (2001) 135–184, https://doi.org/10.1016/S1381-1169(01)00149-2.
[84] R. Dittmeyer, V. Hollein, P. Quicker, G. Emig, G. Hausinger, F. Schmidt, Factors controlling the performance of catalytic dehydrogenation of ethylbenzene in

palladium composite membrane reactors, Chem. Eng. Sci. 54 (10) (1999) 1431–1439, https://doi.org/10.1016/S0009-2509(99)00048-2.
[85] P. Quicker, V. Hollein, R. Dittmeyer, Catalytic dehydrogenation of hydrocarbons in palladium composite membrane reactors, Catal. Today 56 (1–3) (2000) 21–34, https://doi.org/10.1016/S0920-5861(99)00259-X.
[86] N. Itoh, W.-C. Xu, K. Haraya, Basic experimental study on palladium membrane reactors, J. Membr. Sci. 66 (2) (1992) 149–155, https://doi.org/10.1016/0376-7388(92)87005-I.
[87] J.K. Ali, E.J. Newson, D.W.T. Rippin, Deactivation and regeneration of Pd-Ag membranes for dehydrogenation reactions, J. Membr. Sci. 89 (1) (1994) 171–184, https://doi.org/10.1016/0376-7388(93)E0219-A.
[88] R. Dittmeyer, T. Boeltken, P. Piermartini, M. Selinsek, M. Loewert, F. Dallmann, P. Pfeifer, Micro and micro membrane reactors for advanced applications in chemical energy conversion, Curr. Opin. Chem. eng. 17 (2017) 108–125, https://doi.org/10.1016/j.coche.2017.08.001.
[89] T.A. Peters, M. Stange, R. Bredesen, 2 - fabrication of palladium-based membranes by magnetron sputtering, in: A. Doukelis, K. Panopoulos, A. Koumanakos, E. Kakaras (Eds.), Palladium Membrane Technology for Hydrogen Production, Carbon Capture and Other Applications, Woodhead Publishing, 2015, pp. 25–41.
[90] M. De Falco, Membrane reactors modeling, in: M. De De Falco, L. Marrelli, G. Iaquaniello (Eds.), Membrane Reactors for Hydrogen Production Processes, Springer London, London, 2011, pp. 79–102.
[91] T.A. Peters, M. Stange, M.F. Sunding, R. Bredesen, Stability investigation of micro-configured Pd–Ag membrane modules – effect of operating temperature and pressure, Int. J. Hydrogen Energy 40 (8) (2015) 3497–3505, https://doi.org/10.1016/j.ijhydene.2014.11.019.
[92] T.A. Peters, P.A. Carvalho, M. Stange, R. Bredesen, Formation of hydrogen bubbles in Pd-Ag membranes during H2 permeation, Int. J. Hydrogen Energy 45 (12) (2020) 7488–7496, https://doi.org/10.1016/j.ijhydene.2019.02.001.
[93] A. Ramachandran, W.M. Tucho, A.L. Mejdell, M. Stange, H.J. Venvik, J. C. Walmsley, A. Borg, Surface characterization of Pd/Ag23wt% membranes after different thermal treatments, Appl. Surf. Sci. 256 (20) (2010) 6121–6132, https://doi.org/10.1016/j.apsusc.2010.03.131.
[94] W.M. Tucho, H.J. Venvik, M. Stange, J.C. Walmsley, R. Holmestad, R. Bredesen, Effects of thermal activation on hydrogen permeation properties of thin, self-supported Pd/Ag membranes, Separ. Purif. Technol. 68 (3) (2009) 403–410, https://doi.org/10.1016/j.seppur.2009.06.015.
[95] N. Vicinanza, I.H. Svenum, T. Peters, R. Bredesen, H. Venvik, New insight to the effects of heat treatment in air on the permeation properties of thin Pd77%Ag23% membranes, Membranes 8 (4) (2018), https://doi.org/10.3390/membranes8040092.
[96] L. Yang, Z. Zhang, X. Gao, Y. Guo, B. Wang, O. Sakai, T. Takahashi, Changes in hydrogen permeability and surface state of Pd–Ag/ceramic composite membranes after thermal treatment, J. Membr. Sci. 252 (1) (2005) 145–154, https://doi.org/10.1016/j.memsci.2004.12.006.
[97] K. Zhang, S.K. Gade, Ø. Hatlevik, J.D. Way, A sorption rate hypothesis for the increase in H2 permeability of palladium-silver (Pd–Ag) membranes caused by air oxidation, Int. J. Hydrogen Energy 37 (1) (2012) 583–593, https://doi.org/10.1016/j.ijhydene.2011.09.078.
[98] K. Zhang, S.K. Gade, J.D. Way, Effects of heat treatment in air on hydrogen sorption over Pd–Ag and Pd–Au membrane surfaces, J. Membr. Sci. 403–404 (2012) 78–83, https://doi.org/10.1016/j.memsci.2012.02.025.
[99] T.A. Peters, T. Kaleta, M. Stange, R. Bredesen, Hydrogen transport through a selection of thin Pd-alloy membranes: membrane stability, H2S inhibition, and flux recovery in hydrogen and simulated WGS mixtures, Catal. Today 193 (1) (2012) 8–19, https://doi.org/10.1016/j.cattod.2011.12.028.
[100] F. Auer, D. Blaumeiser, T. Bauer, A. Bosmann, N. Szesni, J. Libuda, P. Wasserscheid, Boosting the activity of hydrogen release from liquid organic hydrogen carrier systems by sulfur-additives to Pt on alumina catalysts. [10.1039/C9CY00817A], Catal. Sci. Technol. 9 (13) (2019) 3537–3547, https://doi.org/10.1039/C9CY00817A.
[101] H. Kreuder, Nutzung der Dehydrierung von Methylcyclohexan in mikrostrukturierten Membranreaktoren zur Energiespeicherung: Insititut für Mikroverfahrenstechnik (IMVT), 2017.
[102] I.B. Elkina, J.H. Meldon, Hydrogen transport in palladium membranes, Desalination 147 (1) (2002) 445–448, https://doi.org/10.1016/S0011-9164(02)00641-0.
[103] H. Gabasch, K. Hayek, B. Klotzer, A. Knop-Gericke, R. Schlogl, Carbon incorporation in Pd (111) by adsorption and dehydrogenation of ethene, J. Phys. Chem. B 110 (10) (2006) 4947–4952, https://doi.org/10.1021/jp056765g.
[104] M.W. Tew, M. Nachtegaal, M. Janousch, T. Huthwelker, J.A. van Bokhoven, The irreversible formation of palladium carbide during hydrogenation of 1-pentyne over silica-supported palladium nanoparticles: in situ Pd K and L3 edge XAS, Phys. Chem. Chem. Phys. 14 (16) (2012) 5761–5768, https://doi.org/10.1039/c2cp24068h.
[105] J.J. Velasco-Velez, D. Teschner, F. Girgsdies, M. Havecker, V. Streibel, M. G. Willinger, A. Knop-Gericke, The role of adsorbed and subsurface carbon species for the selective alkyne hydrogenation over a Pd-black catalyst: an operando study of bulk and surface, Top. Catal. 61 (20) (2018) 2052–2061, https://doi.org/10.1007/s11244-018-1071-6.
[106] H. Gao, Y. Lin, Y. Li, B. Zhang, Chemical stability and its improvement of palladium-based metallic membranes, Ind. Eng. Chem. Res. 43 (22) (2004) 6920–6930, https://doi.org/10.1021/ie049722f.
[107] T.A. Peters, W.M. Tucho, A. Ramachandran, M. Stange, J.C. Walmsley, R. Holmestad, R. Bredesen, Thin Pd–23%Ag/stainless steel composite membranes: long-term stability, life-time estimation and post-process characterisation, J. Membr. Sci. 326 (2) (2009) 572–581, https://doi.org/10.1016/j.memsci.2008.10.053.
[108] O.M. Løvvik, S.M. Opalka, Reversed surface segregation in palladium-silver alloys due to hydrogen adsorption, Surf. Sci. 602 (17) (2008) 2840–2844, https://doi.org/10.1016/j.susc.2008.07.016.
[109] A.A.B. Padama, H. Kasai, Y.W. Budhi, Hydrogen absorption and hydrogen-induced reverse segregation in palladium–silver surface, Int. J. Hydrogen Energy 38 (34) (2013) 14715–14724, https://doi.org/10.1016/j.ijhydene.2013.08.138.
[110] I.H. Svenum, J.A. Herron, M. Mavrikakis, H.J. Venvik, Adsorbate-induced segregation in a PdAg membrane model system: Pd3Ag(111), Catal. Today 193 (1) (2012) 111–119, https://doi.org/10.1016/j.cattod.2012.01.007.
[111] N. Vicinanza, I.-H. Svenum, L.N. Næss, T.A. Peters, R. Bredesen, A. Borg, H. J. Venvik, Thickness dependent effects of solubility and surface phenomena on the hydrogen transport properties of sputtered Pd77%Ag23% thin film membranes, J. Membr. Sci. 476 (2015) 602–608, https://doi.org/10.1016/j.memsci.2014.11.031.
[112] T.A. Peters, M. Stange, R. Bredesen, Development of Thin Pd-23% Ag/Stainless Steel Composite Membranes for Application in Water Gas Shift Membrane Reactors Carbon Dioxide Capture for Storage in Deep Geologic Formations–Results from the CO2 Capture Project, 2009, p. 135.

Karlsruher Institut für Technologie

OPEN ACCESS

Repository KITopen

Dies ist ein Postprint/begutachtetes Manuskript.

Empfohlene Zitierung:

Wunsch, A.; Gapp, E.; Peters, T.; Pfeifer, P.
Impact of product gas impurities from dehydrogenation of perhydro-dibenzyltoluene on the performance of a 10 µm PdAg-membrane.
2021. Journal of membrane science, 628
doi:10.5445/IR/1000131024

Zitierung der Originalveröffentlichung:

Wunsch, A.; Gapp, E.; Peters, T.; Pfeifer, P.
Impact of product gas impurities from dehydrogenation of perhydro-dibenzyltoluene on the performance of a 10 µm PdAg-membrane.
2021. Journal of membrane science, 628, Article no: 119094.
doi:10.1016/j.memsci.2021.119094

Lizenzinformationen: KITopen-Lizenz